Linear Diamides Derivative-Nucleated Biodegradable Poly(ethylene succinate) Polyester: Crystallization Kinetics and Aggregated Structure Manipulated by Hydrogen Bond Interaction

Shanshan Zhou
Tianjin University of Technology
Yongyan Sun
Tianjin University of Technology
Huimin Ma
Tianjin University of Technology
Chunfeng Jia
Tianjin University of Technology
Xiaoyu Sun
Tianjin University of Technology
Yubin Yang
Tianjin University of Technology
Juan Liu
Tianjin University of Technology
Jinjun Yang (tjyjj_2014@tjut.edu.cn)
Tianjin University of Technology https://orcid.org/0000-0002-9939-151X

Research Article

Keywords: Polyester, Nucleation, Crystallization, Aggregated structure, Hydrogen bond

Posted Date: February 10th, 2021

DOI: https://doi.org/10.21203/rs.3.rs-169317/v1

Version of Record: A version of this preprint was published at Journal of Polymers and the Environment on April 5th, 2021. See the published version at https://doi.org/10.1007/s10924-021-02141-2.

Abstract

A linear diamides derivative (TMC300) as a nucleating agent (NA) was incorporated into biodegradable poly(ethylene succinate) (PES) to investigate effect of TMC300 on nucleation, crystallizability, crystallization kinetics, aggregated structure of PES. TMC300 enhanced significantly crystallizability and crystallization temperature of PES in cooling process at a rate of 10 ℃/min from molten state, indicating that TMC300 exhibits an excellent nucleation effect on PES. IR measurement suggested that TMC300 interacts with amorphous carbonyl and ester group, and crystalline CH_2 group of PES via hydrogen bond. Change rate of carbonyl group is comparable to that of C—C backbone of PES, regardless of the presence or absence of TMC300. Small difference of diffraction peak in WAXD measurement between neat PES and PES/TMC300 is probably attributed to spherulitic orientation on film surface of neat PES, and different spatial arrangements in the same crystal lattice. TMC300 enhanced carbon residue yield of PES/TMC300 composite, probably related to slight flame retardance effect.

Introduction

Polyester material has attracted more and more interests from scientists, engineers and environmentalists due to its good mechanical properties, biodegradation and biocompatibility (or low toxicity), and is considered as a promising biomaterial to replace traditional petroleum-based plastic with non-biodegradation. It has been widely applied in the medical material, disposable container, food packaging and agricultural film [1–8].

Poly(ethylene succinate) (PES) is a typical linear aliphatic polyester with the biodegradation and its monomer of succinic acid comes from natural resources [9, 10]. It was reported that the PES exhibits comparable mechanical properties to the traditional petroleum-based plastics, such as the polyethylene and polypropylene [9–16] and increasing attention has been paid on the PES. The crystallization behavior, crystallization kinetics and aggregated structure (containing the crystalline structure) significantly influence the physical properties (material density, transparency, mechanical properties and processability), which will further affect the performances (biodegradation, gas barrier, etc.) of the polymeric material. Therefore, the crystallization kinetics and aggregated structure play an important role on the final performance of the polymeric product. The in-depth exploration of the crystallization kinetics and aggregated structure is of scientific importance to tailor the physical properties and performances of the polymeric material. The PES shows the extremely low crystallizability and no discernible crystallization peak can be found in its cooling process (as presented in Fig. 1), resulting in long processing cycle and increased time cost in the processing.

The nucleating agent (NA) as a kind of common filler has been widely applied in the scientific research and material processing due to economy, time saving, efficiency, convenience and eco-friendliness. Upon addition of the heterogenous NA, the polymer molecular chains frequently nucleate on the surface of the NA at a higher temperature and with low free energy, and the crystal growth can be triggered immediately, thus both the crystallization temperature and crystallization rate enhance for the polymeric material. In

the presence of the NA, many polymeric materials exhibit the improved physical properties and tailored performances. To date, many NAs have been incorporated into the PES to manipulate the crystallization/melting behavior, crystal morphology, microstructure and enzymatic hydrolysis rate, enhance thermal stability and improve mechanical properties of the PES [17–27]. Among the NAs aforementioned, some inorganic NAs show the agglomeration morphology and weak interfacial strength/interaction with the PES, resulting in the uncontrolled crystal shape, undesirable or relatively poor physical properties and performances of the composite. By contrast, the organic NA should be a better candidate to increase the interfacial interaction and to realize the uniform dispersion of the NA in the PES matrix.

It was reported that several multiple amides-containing derivatives as the excellent NAs present outstanding nucleation effect via the hydrogen bond interaction. These NAs not only modulate the polymorphism, tailor mechanical properties, increase melt-crystallization temperature (T_c), crystallization rate, degree of crystallinity (X_c), thermal stability and gas barrier performance, but also induce the crystals to self-assemble into the shish-kebab-like (or cone/needle-like) structures of the isotactic polypropylene (iPP) [28–30], poly(L-lactide) (PLLA) [31–41] and poly(1,4-butylene adipate) (PBA) [3, 42–44]. Generally, an excellent NA presents a higher T_c and melting temperature (T_m) than the polymer matrix because the solidified NA crystal can act as the heterogeneous NA on which the molten polymer molecular chains nucleate, before the onset of the crystallization of the polymer [35]. It was documented that the linear multiple amides-based NA with the amide group flanked with the benzene terminal groups, shows a better effect on the nucleation and mechanical properties of the PLLA [41].

Recently, a linear organic derivative (octamethylenedicarboxylic dibenzoylhydrazide (TMC300), see its chemical structure in Scheme 1) bearing the amide groups which are directly linked with the benzene terminal groups, was reported to enhance substantially the T_c and crystallization rate of the bacterially synthesized copolyester, poly(3-hydroxybutyrate-*co*-3-hydroxyhexanoate) (PHBH) [4]. In this work, the TMC300 bearing the multiple amides as a NA was incorporated into the PES to investigate the effect of the TMC300 on the crystallization kinetics and aggregated structure of the PES. It is anticipated that via the hydrogen bond interaction between the PES and amide group of the TMC300, the crystallizability can be enhanced and crystallization process can be accelerated for the PES. In addition, by means of the *in-situ* Fourier transform infrared (FTIR) spectroscopy, the time-dependent aggregated structure of the TMC300-nucleated PES was monitored in the crystallization process, which enables us to follow the evolution of aggregated structure and elucidate the crystallization mechanism of the PES in depth at a molecular level.

Materials And Methods

Materials

The PES was purchased from the Sigma-Aldrich Co., Ltd. (Shanghai, China) and used as received without further purification. The TMC300 was synthesized in our group, and the synthesis method and

procedures refer to the literature [4].

Preparation of the PES/TMC300

The TMC300 was added into the PES-containing chloroform solution and well stirred. After evaporation of the chloroform, the composite sample was transferred into the vacuum oven at 40 ℃ for 5h to remove completely the chloroform. The dried sample was marked as PES/*x*%TMC300, where *x* represents the weight fraction of the TMC300 (f_{TMC300}) in the composite.

Characterization and measurement

Differential scanning calorimetry (DSC). The crystallization and melting curves were recorded on a DSC instrument (PE 4000, U.S.A.). For the non-isothermal crystallization, the sample (5–8 mg) was heated to 190 ℃ and held for 3 min to remove the thermal history, then cooled to -20 ℃ at various rates (2, 5, 10 and 20 ℃/min). Followed by being reheated to 190 ℃. For the isothermal crystallization, the molten sample at 190 ℃ was cooled quickly (with a rate 100 ℃/min) to different T_cs (60, 65, 70 and 75℃) to complete the crystallization process. After the isothermal crystallization, the sample was also reheated to 190 ℃. The DSC data (including the crystallization enthalpy, cold crystallization enthalpy, recrystallization enthalpy and melting enthalpy) were calculated using the unit mass (g) of the sample (J/g).

Polarized optical microscopy (POM). The crystal morphology observation was performed using a POM (XPF550C, Caikon Co. Ltd., Shanghai, China). The sample between 2 glass slides was heated to 190 ℃ to remove the thermal history, and pressed slightly to form a thin film with about 0.05 mm. Eventually, the molten film sample was transferred to a hotstage on which the desirable T_c was set for the isothermal crystallization.

Fourier transform infrared (FTIR) spectroscopy. The FTIR spectrum was collected on an IR instrument (TENSOR 37, Bruker, Germany). The accumulation and resolution are 16 scans and 1 cm^{-1}, respectively. First, the sample placed between 2 KBr discs was heated to 190 ℃ to remove the thermal history, and pressed slightly to form a thin film with about 0.05 mm. Then the sample was transferred to a hotstage preset to the T_c = 25 ℃to complete its isothermal crystallization. For the time-dependent *in-situ* IR measurement, a higher T_c (75 ℃) was set because it allows us to observe the IR spectral alteration real time with a long enough time. The molten film sample at 190 ℃ was transferred rapidly to a hotstage preset to 75 ℃ for a slow isothermal crystallization, and each IR spectrum was collected with a time interval of 2min.

Scanning electron microscopy-energy dispersive spectrometer (SEM-EDS). The N element mapping of the TMC300 in the PES matrix was recorded with a SEM-EDS instrument (SU3500, Hitachi, Japan). The image of the cross section of broken sample was obtained with an acceleration voltage of 30 kV and a working distance of 10–400 mm.

Wide angle X-ray diffraction (WAXD). The crystal structure of the sample was measured on a WAXD instrument (Rigaku Corp., Tokyo, Japan) with Ni-filtered CuKα radiation (λ = 0.154 nm), worked at 40 kV and 200 mA. The sample sandwiched between 2 iron plates was heated to 190 ℃ and held for 3 min to erase the thermal history. Then the molten sample was pressed slightly to form a film with 1 mm and transferred to a hotstage preset to 25 ℃ to complete the isothermal crystallization.

Thermogravimetric analysis (TGA). Thermal stability of the sample was investigated using a TGA instrument (SDT Q600, TA, USA). The sample was heated from the room temperature to 600 ℃ with a rate of 10 ℃/min in the presence of the N_2.

Results And Discussion

Non-isothermal crystallization

The non-isothermal crystallization and subsequent heating curves are presented in Fig. 1. No discernible crystallization peak can be found for neat PES and the T_c of neat TMC300 is about 100 ℃, as shown in Fig. 1a. Upon incorporation of the TMC300, a sharp crystallization peak appeared with the f_{TMC300} = 0.3%, indicating the TMC300 as an effective NA enhanced significantly the crystallizability. With a further increase in the f_{TMC300} (0.5% and 1%), the T_c of the PES changed little, probably ascribed with the saturated effect of the TMC300 NA [4]. In the subsequent heating process, neat PES showed a sharp cold crystallization (cc) peak at T_{cc}, a recrystallization (rc) peak at T_{rc}, and two melting peaks at T_{m1} and T_{m2}, respectively, as presented in Fig. 1b. The cold crystallization peak is an indicative of the rearrangement or adjustment of neat PES molecular chains in the heating process, that is, the insufficient crystallization occurred or the degree of the crystallinity is low for neat PES in the former cooling process. With the loading of the TMC300, no cold crystallization peak can be found, revealing that the TMC300 increased the orderness of the alignment of molecular chains to a certain extent in the cooling process. Multiple melting behaviors of the PES should be attributed to the melting-recrystallization-remelting mechanism, which is widely reported in the polymeric material. The TMC300 exhibited a T_m at about 160 ℃, substantially higher than that of the PES.

The parameters of the thermal property measured using the DSC are summarized in Table 1, where ΔH_c, ΔH_{cc}, ΔH_{rc} and X_c represent the crystallization enthalpy in the cooling process, cold crystallization enthalpy, recrystallization enthalpy in subsequent heating process and relative degree of the crystallinity, respectively. The X_c value refers to the ratio of $\Delta H_m'$ and ΔH_m^0 (($\Delta H_m'/\Delta H_m^0$)×100%), and $\Delta H_m'$ = (ΔH_m + ΔH_{cc}+ ΔH_{rc}) and ΔH_m^0 is ΔH_m of an infinitely large crystal of the PES. It was documented that the ΔH_m^0 value of the PES is 180 J/g [15]. The X_c value of the PES enhanced markedly in the presence of the TMC300, but a slight increase in the X_c value can be found for three PES/TMC300 composites (with the f_{TMC300} = 0.3-1%), confirming again that the nucleation of the PES tends to saturation with the higher f_{TMC300}. To the best of our knowledge, the ΔH_m^0 value of the TMC300 is unavailable.

The non-isothermal DSC curves at various rates are presented in Fig. S1 (Supplementary Material). With an increase in the cooling rate, the T_c of the PES decreased, suggesting that the lower cooling rate is favorable for the nucleation and crystallization of the PES. No crystallization peak could be found for neat PES when the cooling rate is 10 or 20 ℃/min, indicating that the difficulty in the crystallization for neat PES. The DSC data in the cooling process from the molten state at the rates of 2, 5 and 20 ℃/min, respectively, are shown in Table S1 (Supplementary Material). On the whole, both the T_c and the absolute value of the ΔH_c of the PES increased slightly with the f_{TMC300}, at the same cooling rate.

Table 1
DSC data in non-isothermal cooling and subsequent heating process. Both cooling and heating rate are 10°C/min

Sample	Cooling		Heating						PES X_c/%
	T_c (°C)	$-\Delta H_c$ (J/g)	T_{cc} (°C)	$-\Delta H_{cc}$ (J/g)	T_{rc} (°C)	$-\Delta H_{rc}$ (J/g)	T_m (°C)	ΔH_m (J/g)	
PES	N.P.	0	33.3	38.9	70.5	10.5	85.4, 99.1	79.8	16.9
PES/0.3%EBH	61.5	46.7	N.P.	0	81.4	8.2	89.8, 98.5	72.7	35.8
PES/0.5%EBH	62.8	49.2	N.P.	0	82.0	9.1	90.4, 97.9	75.3	36.7
PES/1%EBH	62.8	49.6	N.P.	0	82.9	8.6	90.7, 99.3	76.9	37.9
EBH	100.3	30.9	N.P.	0	N.P.	0	161.7	36.2	—

N.P., no peak is discernible; —, no data are available.

Isothermal crystallization and crystallization kinetics

Isothermal crystallization curves of neat PES and PES/TMC300 at different T_cs (60, 65, 70 and 75 ℃), are shown in Fig. 2. No obvious crystallization peak is discernible for neat PES. However, with addition of the TMC300, the sharp crystallization peak of the PES appeared and it narrowed much with an increase in the f_{TMC300}. In addition, the crystallization time decreased largely in the presence of the TMC300, reflecting that the TMC300 is indeed an excellent NA on the PES.

For quantitative analysis of the crystallization kinetics of neat PES and PES/TMC300 at different T_cs, modified method and guideline based on Avrami Equation were adopted [45–48]. Figure 3 shows the X_t as a function of the crystallization time (t), in which the X_t represents the relative degree of the crystallinity at the time t. All these plots present the “S” shapes. Obviously, at the same t, the PES exhibited much higher crystallinity in the presence of the TMC300, and the TMC300 shortened substantially the crystallization time at which 100% crystallinity is achieved. The Avrami plots are shown in Fig. 4, and good linear fitting with correlation coefficient higher than 0.991 was obtained in each plot

and their slopes are close to each other. The crystallization kinetics parameters of neat PES and PES/TMC300 at different T_cs, are listed in Table 2. $t_{1/2}$ is the crystalliztion hafe-time at which the relative degree of the crystalinity is 50%. n is the Avrami exoponent ralated to both the nucleation manner (homogeneous or heterogeneous, n_1) and crystal growth dimension (n_2). $n = n_1 + n_2$ and n_1 equals to 1 in the case of homogeneous nucleation or 0 in the case of heterogeneous nucleation. k is the crystallization rate constant which is influenced by both the nucleation and crystal growth. Clearly, the $t_{1/2}$ depressed significantly and k increased substantially with the loading of the TMC300, indicating that the crystallization rate of the PES enhanced largely in the presence of the TMC300. In terms of n, neat PES is close to 3 (instead of 4), seemingly suggest that neat PES exhibits 2-dimensional crystal ($n_1 = 1$ and $n_2 = 2$). However, from the POM image in Fig. 5a, neat PES showed the typical 3-dimensinal spherulites not 2-dimensional crystal. It probably is ascribed with some impurities in the PES. With an increase in the f_{TMC300}, n declined gradually to 2, suggesting that the morphology transition from the 3D spherulite in neat PES to 2D shape in the PES/TMC300. Due to some uncertainties, calculated n value is not an integer.

Table 2
Calculated crystallization kinetics parameters of PES and PES/TMC300 at various T_cs

T_c/°C	Sample	$t_{1/2}$/min	n	k/min^{-n}
60	PES	6.20	3.0	2.9×10^{-3}
	PES/0.3%TMC300	0.34	2.9	15.8
	PES/0.5%TMC300	0.32	2.8	16.8
	PES/1%TMC300	0.28	2.6	19.0
65	PES	10.1	3.1	5.3×10^{-4}
	PES/0.3%TMC300	0.61	2.8	2.8
	PES/0.5%TMC300	0.46	2.4	4.5
	PES/1%TMC300	0.25	2.2	14.6
70	PES	11.2	2.9	6.3×10^{-4}
	PES/0.3%TMC300	1.88	2.8	0.12
	PES/0.5%TMC300	1.09	2.6	0.55
	PES/1%TMC300	0.57	2.2	2.39
75	PES	12.7	2.9	4.4×10^{-4}
	PES/0.3%TMC300	5.40	2.7	1.1×10^{-2}
	PES/0.5%TMC300	4.31	2.4	2.1×10^{-2}
	PES/1%TMC300	1.51	2.1	0.30

Crystal morphology observation

65 ℃ as an example was chosen a T_c to observe the crystal morphology. Neat PES presented a large spherulite at 65 ℃ (Fig. 5a) and, the crystal size decreased markedly and crystal density increased significantly with the loading of the TMC300, especially in the PES/1%TMC300 (Fig. 5d). It indicates that the TMC300 showed the outstanding nucleation effect on the PES.

Hydrogen bond interaction measured by IR

Figure 6 shows the IR spectra (panels a and c) of neat PES, TMC300 and PES/TMC300 at T_c = 25 ℃ in two wavenumber regions. For clear distinguishing of subtle difference, the corresponding 2nd derivatives of the IR spectra are also presented in Fig. 6 (panels b and d). Neat PES showed the IR absorption peaks at 1730 and 1774 cm^{-1}, attributed to the carbonyl (C = O) group in the crystalline (denote as “C = O cry.” in

Fig. 6a) and amorphous (denote as “C = O amo.” in Fig. 6a) phase [49–51], respectively. No IR peak could be found for neat TMC300 in the region of 1800 – 1700 cm^{-1}. With incorporation of the TMC300, the peak at 1774 cm^{-1} shifted to 1770 cm^{-1} (as presented in Fig. 6b) and that at 1730 cm^{-1} changed little, suggesting that the TMC300 (–NH– or $–CH_2–$ group) interacts with the C = O group of the amorphous phase of the PES. An IR peak at 1605 cm^{-1} is assigned to the amide (O = C–NH–) group [52] of the TMC300 and it moved to a lower wavenumber region (1601 cm^{-1}), indicating that the amide group of the TMC300 interacts with the PES ($–CH_2–$/$–CH_3–$ group). The IR peak at 1116 cm^{-1} is associated with the ester (O = C–O–C) group of the PES and it moved gradually to 1122 cm^{-1} with an increase in the f_{TMC300}, as shown in Figs. 6c and d, reflecting that the hydrogen bond interaction also exists between the ester of the PES and TMC300.

Possible nucleation mechanism

The nucleation mechanism of the polymer in the presence of the NA can mainly be attributed to the chemical nucleation and epitaxial nucleation [53, 54]. Chemical nucleation can be described as follows. In the sample preparation process, the chemical reaction between the polymer and NA occurs and newly formed substance can act as the NA of the polymer. In this case, there is an extremely low possibility that chemical reaction between the PES and TMC300 occurred. Epitaxial nucleation refers to good matching of the crystal lattice between the polymer and NA. To the best of our knowledge, no data on the crystal lattice sizes of the TMC300 is available at present. It is difficult that to confirm that whether or not there is good crystal lattice matching between the PES and TMC300.

It was documented that the uniform dispersion of the multiple wall carbon nanotube (MWNT) enhances greatly the nucleation and crystallizability of the poly(□-caprolactone) (PCL) and the superfine MWNT NA exhibits the supernucleation effect on the PCL [55]. Authors speculates that the homogeneously/evenly distribution of the MWNT is an important factor leading to the nucleation of the PCL. In this work, the hydrogen bond interaction between the PES and TMC300 is favorable for good dispersion of the TMC300 in the PES matrix, which induced the nucleation of the PES.

Time-dependent in-situ FTIR

For real-time observation of spectra change, time-dependent FTIR spectra of neat PES and PES/1%TMC300 collected at 75 ℃, are shown in Fig. 7. From Fig. 7a, the intensity of most of IR peaks (at 1734, 1450, 1415, 1379, 1349, 1314, 1046, 971, 924 and 872 cm^{-1}) increased with the crystallization time and these peaks are considered as the crystalline peaks (denoted as the ↑ arrow). The intensity of an IR peak at 1146 cm^{-1} decreased with the crystallization time and it is an amorphous peak (denoted as the ↓ arrow). With loading of the TMC300, two new IR absorption peaks between 1620 and 1550 cm^{-1} appeared, related to the amide group of the TMC300. These two peaks are the crystalline one because they enhanced in their peak intensities. In addition, the peak shift occurred for 3 peaks in the presence of the TMC300, that is, 1415 cm^{-1}◊1422 cm^{-1}, 1146 cm^{-1}◊1152 cm^{-1} and 1046 cm^{-1}◊1040 cm^{-1}, respectively. The intensity variation and peak shift should be ascribed with the reorganization/adjustment

of the molecular chains of the PES in the crystallization process. Based on the previous literatures on the polyester [56–59], the IR peaks assignment of the PES is summarized as follows. The peak at 1734 cm^{-1} is assigned to the carbonyl stretching mode, and those in 1500–1400 and 1400 – 1300 cm^{-1} are ascribed with the CH_2 bending and wagging mode, respectively. Peaks in the wavenumber of 1300 – 1100 cm^{-1} are attributed to the ester stretching mode. Those in 1100 – 1000 cm^{-1} are related to C–C backbone stretching mode. IR peaks in 1000 – 800 cm^{-1} are assigned to CH_2 rocking mode. It should be mentioned that the positions of the carbonyl and ester group in Fig. 7 differ from those in Fig. 6, probably resulted from the variation in the T_c.

With combination of IR results from Figs. 6 and 7, the hydrogen bond interaction formed between the PES and TMC300 is illustrated in Fig. 8. The TMC300 interacted with the carbonyl and ester group in the PES amorphous phase, and with the CH_2 group in the PES crystalline phase.

For direct comparison of the crystallization rate, the normalized intensity of several IR characteristic peaks (assigned to the carbonyl, ester and C–C group, respectively) as the crystallization time, are plotted, as shown in Fig. 9. The peak intensity of the carbonyl and ester group increased with the time, but that of the ester group depressed. Clearly, by contrast, the intensity change of these 3 IR peaks accelerated substantially with loading of the TMC300, revealing that the TMC300 enhanced highly the crystallization rate of the PES. The variation rate of the carbonyl group was comparable to that of the C–C backbone, regardless of the presence or absence of the TMC300.

Crystal structure measurement by WAXD

The WAXD patterns of neat PES, TMC300 and PES/TMC300 at T_c = 25 ℃ are presented in Fig. 10. Neat PES showed two main peaks assigned to the diffraction planes (021) and (200) [14]. With loading of the TMC300, a weak should peak assigned to the diffraction planes (121) of the PES [20] could be found. Absence of this should peak in neat PES is probably attributed to its significantly large crystal (as presented in Fig. 5a), resulted in the orientation of neat PES spherulite on the film surface. Similar results have been reported in poly[(3-hydroxybutyrate)-co-(3-hydroxyhexanoate)] [60], poly(3-hydroxybutyrate) [61] and poly(ethylene adipate) [62]. It is noteworthy that there was an obvious difference in the peak intensity ratio between (021) and (200), that is, I(021)/I(200), for neat PES and PES/TMC300, probably ascribed with different spatial arrangements in the same crystal lattice [63–65]. Hence, the TMC300 had little effect on the crystal structure of the PES.

Thermal stability by TGA

The mass and derivative mass as a function of the temperature are shown in Fig. 11. The mass loss of the sample occurred mainly in the temperature range of 300–455 ℃. From Fig. 11a (TGA curves), both neat PES and PES/TMC300 presented one-step decomposition behavior, but neat TMC300 showed two-step decomposition one, which could be clearly seen in the DTG curves in Fig. 11b (peaks 1 and 2). From 300 to 370 ℃, the order of the thermal degradation temperature is: neat PES > PES/TMC300 > neat TMC300. From 425 to 455 ℃, the thermal degradation temperature of neat TMC300 is higher than those

of neat PES and PES/TMC300. In addition, the residue yield of neat PES is lower than those of neat TMC300 and PES/TMC300 at 600 ℃. The mass loss of neat TMC300 in the first stage (peak 1) is probably attributed to the evaporation of formed NH_3 and H_2O gases in a lower temperature region, and that in the second stage (peak 2) should be associated with the escape of the gases related to the decomposition of the benzene ring and C–C backbone in a relatively higher temperature region. The decomposition of neat PES and PES/TMC300 are mainly ascribed with the developed H_2O, CO and CO_2, and other low molecular weight gases containing the carbonyl and hydroxy groups. With comparison of neat PES, the enhanced carbon residue yield in neat TMC300 and PES/TMC300 are probably related to the slight flame retardance effect of the TMC300. It was reported that many organic substances with the N or P element (as the excellent flame retardant) increased the flame retardance or fire resistance of the polymeric composites, because these flame retardants migrate to the surface of the polymeric material and react with the polymer to form a thin carbon layer (with a lower heat conductivity) to prevent from the direct contact with the heat flow [66, 67].

Conclusion

No discernible crystallization peak could be found for neat PES, but the PES/TMC300 showed a sharp crystallization peak, suggesting that the TMC300 increased highly the crystallizability of the PES. The TMC300 enhanced substantially the crystallization rate and shortened significantly the crystallization time of the PES, indicating that the TMC300 is a good nucleating agent of the PES. IR investigation revealed that the hydrogen bond exists between the TMC300 and the amorphous carbonyl and ester group, and crystalline CH_2 group of the PES. Absence of the weak (121) diffraction peak of neat PES is probably attributed to the spherulitic orientation on neat PES film surface. The difference of $I(021)/I(200)$ between neat PES and PES/TMC300 should be ascribed with different spatial arrangements in the same crystal lattice.

Declarations

Author contribution statement

The main experiments were conducted and this article was written by Shanshan Zhou. Data collection and processing were performed by Yongyan Sun, Huimin Ma, Chunfeng Jia, Xiaoyu Sun and Yubin Yang. Both Jinjun Yang and Juan Liu contributed to the design of the experiments, analysis of the data and revision of the manuscript.

Declaration of competing interest

The authors declare no competing financial interest.

Acknowledgements

This work was financially supported by the “Natural Science Foundation of Tianjin City (20JCYBJC00580)”, “Program for Prominent Young College Teachers of Tianjin Educational Committee”, “Open Fund of Key Laboratory of Original Agro-Environmental Pollution Prevention and Control (18nybcdhj-4)” and “Training Program for Innovative Research Team in Tianjin Institutions of Higher Education (TD13-5021)”.

References

1. Papageorgiou GZ, Bikiaris DN (2009) Synthesis and properties of novel biodegradable/biocompatible poly[propyleneco-(ethylene succinate)] random copolyesters. Macromol Chem Phys 210:1408–1421
2. Qu D, Zhang F, Gao H, Wang Q, Bai Y, Liu H (2019) Studies on isosorbide-enhanced biodegradable poly(ethylene succinate). Chem Res Chinese U 35:345–352
3. Li L, Tang J, Li Y, Yang J, Sun Y, Ma H, Zhou S, Zhang C, Wang X (2020) Multiple amides derivative-nucleated poly(1,4-butylene adipate) polyester: Tailored temperature-dependent polymorphism, crystal morphology and phase transition. Polymer 186:122088
4. Li L, Yang L, Tang J, Yang J, Li W, Zhou S, Ma H, Zhu H, Zhu Z (2020) Modulated crystallization behavior of bacterial copolyester poly(3-hydroxybutyrate-co-3-hydroxyhexanoate): Effect of a linear multiple amides derivative as a nucleator. J Macromol Sci A 57:439–450
5. Yang J, Wang X, Liang R, Kong R, Sun Y, Tang J, Li L, Xue L, Chen Q (2018) Polymorphism, thermal stability and enzymatic degradation of poly(1,4-butylene adipate) tailored by a benzene-1,3,5-tricarboxamide-based nucleating agent. J Mater Sci 53:10569–10581
6. Hua L, Chen Q, Yin J, Zhang C, Wang X, Feng X, Yang J (2017) Fabrication and physical properties of poly(e-caprolactone)/modified graphene nanocomposite. Macromol Mater Eng 302:1600328–1600338
7. Yang J, Cao X, Zhao Y, Wang L, Liu B, Jia J, Liang H, Chen M (2017) Enhanced pH stability, cell viability and reduced degradation rate of poly(L-lactide)-based composite in vitro: Effect of modified magnesium oxide nanoparticles. J Biomater Sci Polym E 28:488–503
8. Liang R, Chen Y, Zhang C, Yin J, Liu X, Wang L, Kong R, Feng X, Yang J (2017) Crystallization behavior of biodegradable poly(ethylene adipate) modulated by a benign nucleating agent: zinc phenylphosphonate. Chinese J Polym Sci 35:558–568
9. Qiu S, Zhang K, Su Z, Qiu Z (2018) Thermal behavior, mechanical and rheological properties, and hydrolytic degradation of novel branched biodegradable poly(ethylene succinate) copolymers. Polym Test 66:64–69
10. Zhang K, Qiu Z (2019) Miscibility and crystallization behavior of novel branched poly(ethylene succinate)/poly(vinyl phenol) blends. Chinese J Polym Sci 37:1169–1175

11. Ishii N, Inoue Y, Shimada K, Tezuka Y, Mitomo H, Kasuya K (2007) Fungal degradation of poly(ethylene succinate). Polym Degrad Stab 94:44–52
12. Ichikawa Y, Washiyama J, Moteki Y, Noguchi K (1995) Crystal modification in poly(ethylene succinate). Polymer 27:1264–1266
13. Tezuka Y, Ishii N, Kasuya K, Mitomo H (2004) Degradation of poly(ethylene succinate) by mesophilic bacteria. Polym Degrad Stab 84:115–121
14. Ueda A, Chatani Y, Tadokoro H (1971) Structure studies of polyesters. . molecular and structure of poly(ethylene succinate) and poly(ethylene oxalate). Polym J 2:387–397
15. Papageorgiou GZ, Bikiaris DN (2005) Crystallization and melting behavior of three biodegradable poly(alkylene succinates). A comparative study. Polymer 46:12081–12092
16. Zhao J, Wang X, Zhou W, Zhi E, Zhang W, Ji J (2013) Graphene-reinforced biodegradable poly(ethylene succinate) nanocomposites prepared by *in situ* polymerization. J Appl Polym Sci 130:3212–3220
17. Ray SS, Makhatha ME (2009) Thermal properties of poly(ethylene succinate) nanocomposite. Polymer 50:4635–4643
18. Bandyopadhyay J, Ray SS, Scriba M, Malwela T (2012) The impact of nanoclay on the crystal growth kinetics and morphology of biodegradable poly(ethylene succinate) composite. Polymer 53:3602–3612
19. Papageorgiou GZ, Terzopoulou Z, Achilias DS, Bikiaris DN, Kapnisti M, Gournis D (2013) Biodegradable poly(ethylene succinate) nanocomposites. Effect of filler type on thermal behaviour and crystallization kinetics. Polymer 54:4604–4616
20. Asadinezhad A, Khonakdar HA, Häußler L, Wagenknecht U, Heinrich G (2014) Crystallization and melting behavior of poly (ethylene succinate) in presence of graphene nanoplatelets. Thermochim Acta 586:17–24
21. Papageorgiou GZ, Terzopoulou Z, Tsanaktsis V, Achilias DS, Triantafyllidis K, Diamanti EK, Gournis D, Bikiaris DN (2015) Effect of graphene oxide and its modification on the microstructure, thermal properties and enzymatic hydrolysis of poly(ethylene succinate) nanocomposites. Thermochim Acta 614:116–128
22. Zhu S, Zhao Y, Qiu Z (2011) Crystallization kinetics and morphology studies of biodegradable poly(ethylene succinate)/multi-walled carbon nanotubes nanocomposites. Thermochim Acta 517:74–80
23. Teng S, Qiu Z (2017) Enhanced crystallization and mechanical properties of biodegradablepoly(ethylene succinate) by octaisobutyl-polyhedral oligomericsilsesquioxanes in their nanocomposites. Thermochim Acta 649:22–30
24. Tang L, Qiu Z (2016) Effect of poly(ethylene glycol)-polyhedral oligomeric silsesquioxanes on the crystallization kinetics and morphology of biodegradable poly(ethylene succinate). Polym Degrad Stab 134:97–104

25. Asadinezhad A, Khonakdar HA, Scheffler C, Wagenknecht U, Heinrich G (2013) Poly(ethylene succinate)/single-walled carbon nanotube composites: a study on crystallization. Polym Bull 70:3463–3474
26. Asadi V, Jafari SH, Khonakdar HA, Häußler L, Wagenknecht U (2016) Incorporation of inorganic fullerene-like WS_2 into poly(ethylene succinate) to prepare novel biodegradable nanocomposites: a study on isothermal and dynamic crystallization. RSC Adv 6:4925–4935
27. Jing X, Qiu Z (2014) Influence of thermally reduced graphene low-loadings on the crystallization behavior and morphology of biodegradable poly(ethylene succinate). Ind Eng Chem Res 53:498–504
28. Varga József, Menyhárd Alfréd (2007) Effect of solubility and nucleating duality of *N*,*N*′-dicyclohexyl-2,6-naphthalenedicarboxamide on the supermolecular structure of isotactic polypropylene. Macromolecules 40:2422-2431
29. Bai H, Wang Y, Zhang Z, Han L, Li Y, Liu L, Zhou Z, Men Y (2009) Influence of annealing on microstructure and mechanical properties of isotactic polypropylene with β-phase nucleating agent. Macromolecules 42:6647–6655
30. Chen Y, Zhong G, Wang Y, Li Z, Li L (2009) Unusual tuning of mechanical properties of isotactic polypropylene using counteraction of shear flow and β-nucleating agent on β-form nucleation. Macromolecules 42:4343–4348
31. Kawamoto N, Sakai A, Horikoshi T, Urushihara T, Tobita E (2006) Nucleating agent for poly(L-lactic acid)–an optimization of chemical structure of hydrazide compound for advanced nucleation ability. J Appl Polym Sci 103:198–203
32. Xie Q, Han L, Shan G, Bao Y, Pan P (2016) Polymorphic crystalline structure and crystal morphology of enantiomeric poly(lactic acid) blends tailored by a self-assemblable aryl amide nucleator. ACS Sustain Chem Eng 4:2680–2688
33. Kawamoto N, Sakai A, Horikoshi T, Urushihara T, Tobita E (2007) Physical and mechanical properties of poly(L-lactic acid) nucleated by dibenzoylhydrazide compound. J Appl Polym Sci 103:244–250
34. Xu T, Zhang A, Zhao Y, Han Z, Xue L (2015) Crystallization kinetics and morphology of biodegradable poly(lactic acid) with a hydrazide nucleating agent. Polym Test 45:101–106
35. Ma P, Xu Y, Shen T, Dong W, Chen M, Lemstra PJ (2015) Tailoring the crystallization behavior of poly(L-lactide) with self-sssembly-type oxalamide compounds as nucleators: 1. Effect of terminal configuration of the nucleators. Eur Polym J 70:400–411
36. Ma P, Xu Y, Wang D, Dong W, Chen M (2014) Rapid crystallization of poly(lactic acid) by using tailor-made oxalamide derivatives as novel soluble-type nucleating agents. Ind Eng Chem Res 53:12888–12892
37. Xiong Z, Zhang X, Wang R, Vos S de, Wang R, Joziasse CAP, Wang D (2015) Favorable formation of stereocomplex crystals in poly(L-lactide)/poly(D-lactide) blends by selective nucleation. Polymer 76:98–104
38. Bai H, Zhang W, Deng H, Zhang Q, Fu Q (2011) Control of crystal morphology in poly (L-lactide) by adding nucleating agent. Macromolecules 44:1233–1237

39. Xing Q, Li R, Dong X, Luo F, Kuang X, Wang D, Zhang L (2015) Enhanced crystallization rate of poly(L-lactide) mediated by a hydrazide compound: nucleating mechanism study. Macromol Chem Phys 216:1134–1145
40. Fan Y, Zhu J, Yan S, Chen X, Yin J (2015) Nucleating effect and crystal morphology controlling based on binary phase behavior between organic nucleating agent and poly(L-lactic acid). Polymer 67:63–71
41. Bai H, Huang C, Xiu H, Zhang Q, Deng H, Wang K, Chen F, Fu Q (2014) Significantly improving oxygen barrier properties of polylactide via constructing parallel-aligned shish-kebab-like crystals with well-interlocked boundaries. Biomacromolecules 15:1507–1514
42. Kong R, Jia Y, Yang J, Wang X, Sun Y, Lian J, Chen J, Kuang Y, Li Y, Huang M (2019) Polymorphism and properties of biodegradable poly(1,4-butylene adipate) tailored by an aliphatic diamide derivative. Polym Int 68:351–359
43. Yang J, Liang R, Kong R, Chen Y, Wang X, Yin J, Wan J, Wang X, Bi C (2017) Crystal morphology, crystallization behavior, polymorphic crystalline structure and thermal stability of poly(1,4-butylene adipate) modulated by a oxalamide derivative nucleating agent. Polym Degrad Stab 144:33–42
44. Yang J, Liang R, Chen Y, Zhang C, Zhang R, Wang X, Kong R, Chen Q (2017) Using a Self-assemblable nucleating agent to tailor crystallization behavior, crystal morphology, polymorphic crystalline structure and biodegradability of poly(1,4-butylene adipate). Ind Eng Chem Res 56:7910–7919
45. Fillon B, Wittmann JC, Lotz B, Thierry A (1993) Self-nucleation and recrystallization of isotactic polypropylene (α phase) investigated by differential scanning calorimetry. J Polym Sci Polym Phys 31:1383–1393
46. Fillon B, Lotz B, Thierry A, Wittmann JC (1993) Self-nucleation and enhanced nucleation of polymers. Definition of a convenient calorimetric “efficiency scale” and evaluation of nucleating additives in isotactic polypropylene (α phase). J Polym Sci Polym Phys 31:1395–1405
47. Trujillo M, Arnal ML, Müller AJ, Laredo E, Bredeau St, Bonduel D, Dubois Ph (2007) Thermal and morphological characterization of nanocomposites prepared by in-situ polymerization of high-density polyethylene on carbon nanotubes. Macromolecules 40:6268–6276
48. Müller AJ, Arnal ML, Trujillo M, Lorenzo AT (2011) Super-nucleation in nanocomposites and confinement effects on the crystallizable components within block copolymers, miktoarm star copolymers and nanocomposites. Eur Polym J 47:614–629
49. Suttiwijitpukdee N, Sato H, Zhang J, Hashimoto T, Ozaki Y (2011) Intermolecular interactions and crystallization behaviors of biodegradable polymer blends between poly(3-hydroxybutyrate) and cellulose acetate butyrate studied by DSC, FT-IR, and WAXD. Polymer 52:461–471
50. Khasanah, Reddy KR, Sato H, Takahashi I, Ozaki Y (2015) Intermolecular hydrogen bondings in the poly(3-hydroxybutyrate) and chitin blends: Their effects on the crystallization behavior and crystal structure of poly(3-hydroxybutyrate). Polymer 75:141–150

51. Marlina D, Hoshina H, Ozaki Y, Sato H (2019) Crystallization and crystalline dynamics of poly(3-hydroxybutyrate)/poly(4-vinylphenol) polymer blends studied by low-frequency vibrational spectroscopy. Polymer 181:121790
52. Rastogi VK, Singh C, Jain V, Palafox MA (2000) FTIR and FT-Raman spectra of 5-methyluracil (thymine). J Raman Spectrosc 31:1005–1012
53. Legras R, Mercie JP, Nield E (1983) Polymer crystallization by chemical nucleation. Nature 304:432–434
54. Okada K, Watanabe K, Urushihara T, Toda A, Hikosaka M (2007) Role of epitaxy of nucleating agent (NA) in nucleation mechanism of polymers. Polymer 48:401–408
55. Trujillo M, Arnal ML, Müller AJ, Mujica MA, Navarro CU de, Ruelle B, Dubois P (2012) Supernucleation and crystallization regime change provoked by MWNT addition to poly(□-caprolactone). Polymer 53:832–841
56. Yang J, Li Z, Pan P, Zhu B, Dong T, Inoue Y (2009) Temperature-dependent polymorphic crystalline structure and melting behavior of poly(butylene adipate) investigated by time-resolved FTIR spectroscopy. J Polym Sci Part B 47:1997–2007
57. Zhang J, Sato H, Noda I, Ozaki Y (2005) Conformation rearrangement and molecular dynamics of poly(3-hydroxybutyrate) during the melt-crystallization process investigated by infrared and two-dimensional infrared correlation spectroscopy. Macromolecules 38:4274–4281
58. Pan P, Kai W, Zhu B, Dong T, Inoue Y (2007) Polymorphous crystallization and multiple melting behavior of poly(l-lactide): Molecular weight dependence. Macromolecules 40:6898–6905
59. Zhu B, He Y, Asakawa N, Yoshie N, Nishida N, Iuoue Y (2005) Polymorphic crystallization and melting–recrystallization behavior of poly(3-hydroxypropionate). Macromolecules 38:6455–6465
60. Pan P, Liang Z, Nakamura N, Miyagawa T, Inoue Y (2009) Uracil as nucleating agent for bacterial poly[(3-hydroxybutyrate)-co-(3-hydroxyhexanoate)] copolymers. Macromol Biosci 9:585–595
61. Gazzano M, Tomasi G, Scandola M (1997) X-ray investigation on melt-crystallized bacterial poly(3-hydroxybutyrate). Macromol Chem Phys 198:71–80.
62. Yang J, Pan P, Dong T, Inoue Y (2010) Crystallization kinetics and crystalline structure of biodegradable poly(ethylene adipate). Polymer 51:807–815
63. Jiang N, Zhao L, Gan Z (2010) Influence of nucleating agent on the formation and enzymatic degradation of poly(butylene adipate) polymorphic crystals. Polym Degrad Stab 95:1045–1053
64. Chen Y, Wang S, Chen Q, Xi Z, Wang C, Chen X, Feng X, Liang R, Yang J (2015) Modulated crystallization behavior, polymorphic crystalline structure and enzymatic degradation of poly(butylene adipate): Effects of layered metal phosphonate. Eur Polym J 72:222–237
65. Tang Y, Xu J, Guo B (2015) Polymorphic behavior and enzymatic degradation of poly(butylene adipate) in the presence of hexagonal boron nitride nanosheets. Ind Eng Chem Res 54:1832–1841
66. Shen D, Xu Y, Long J, Shi X, Chen L, Wang Y (2017) Epoxy resin flame-retarded via a novel melamine-organophosphinic acid salt: Thermal stability, flame retardance and pyrolysis behavior. J Anal Appl

Pyrol 128:54–63

67. Qiu S, Xing W, Feng X, Yu B, Mu X, Yuen RKK, Hu Y (2017) Self-standing cuprous oxide nanoparticles on silica@polyphosphazene nanospheres: 3D nanostructure for enhancing the flame retardancy and toxic effluents elimination of epoxy resins via synergistic catalytic effect. Chem Eng J 309:802–814

Figures

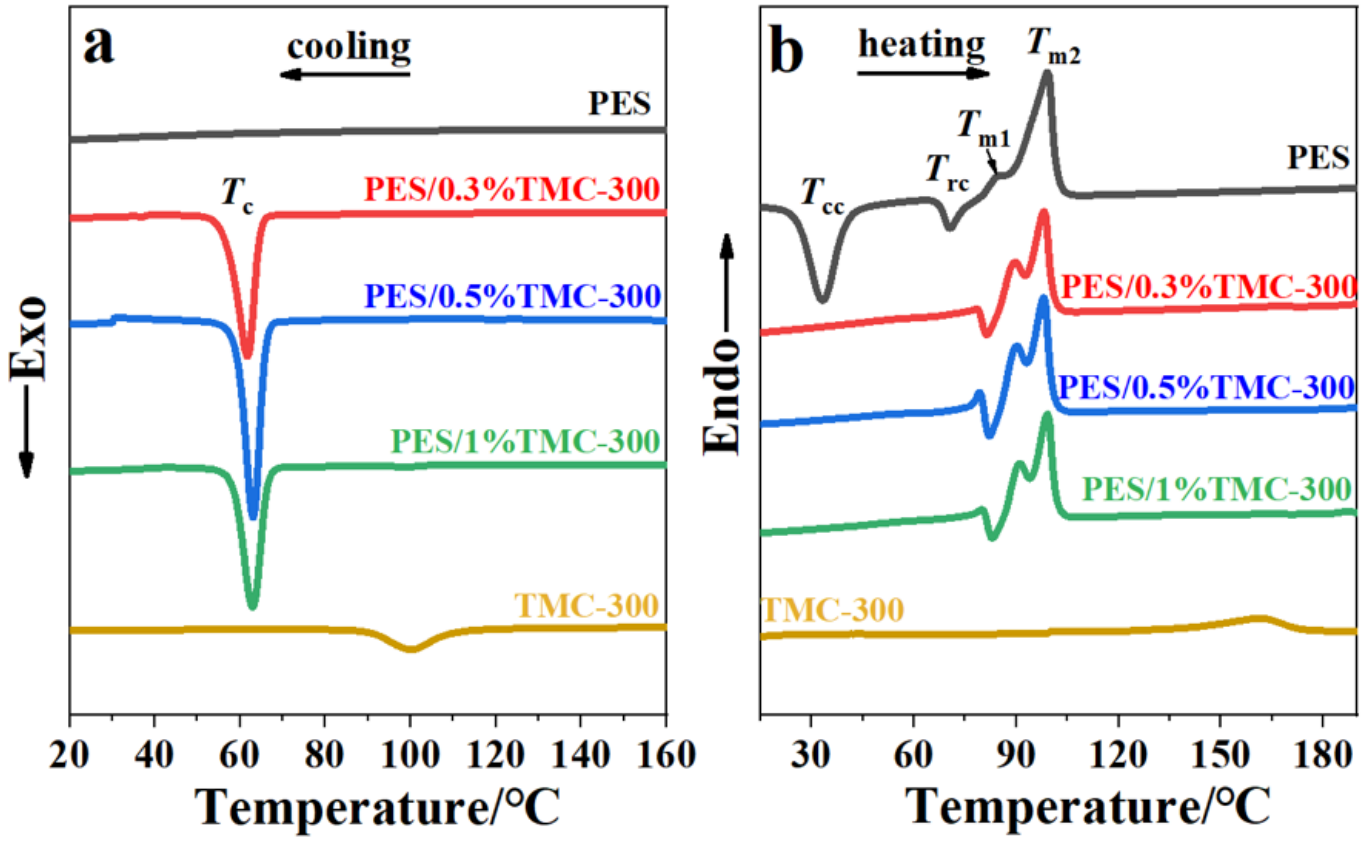

Figure 1

Non-isothermal cooling (a) and subsequent heating (b) DSC curves. Both cooling and heating rates are 10 °C/min

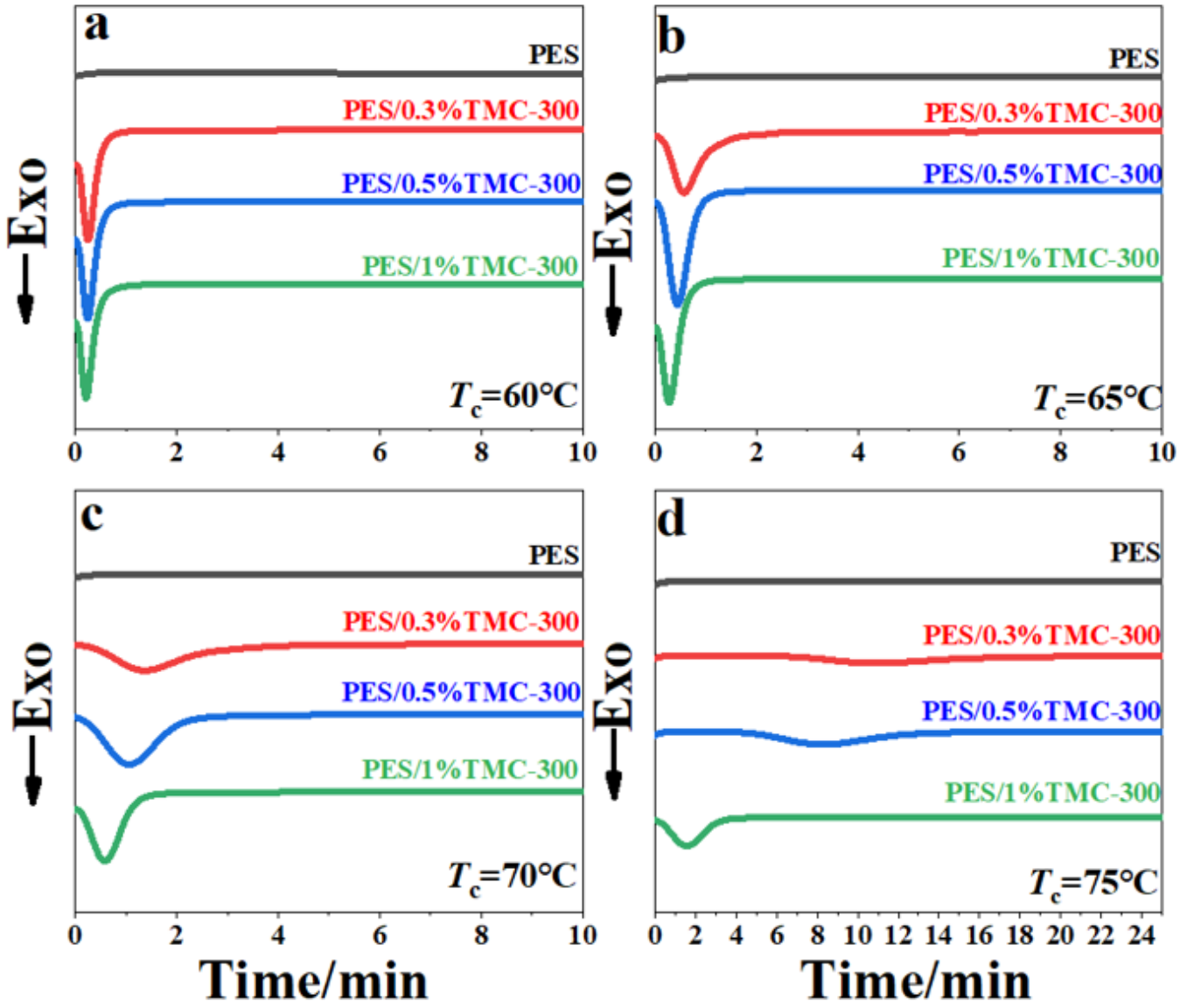

Figure 2

Isothermal crystallization DSC curves at different Tcs

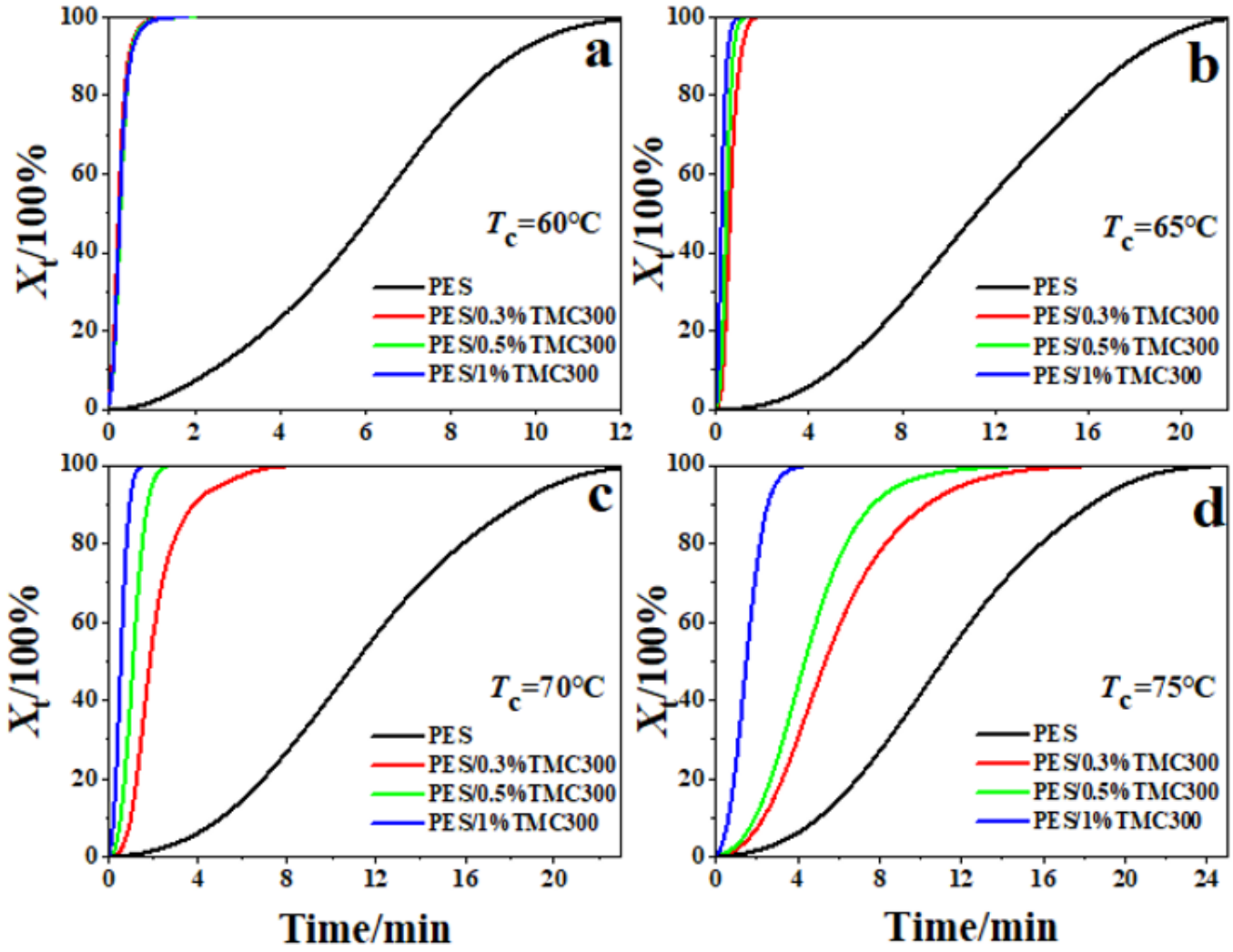

Figure 3

The Xt as a function of the crystallization time at different Tcs

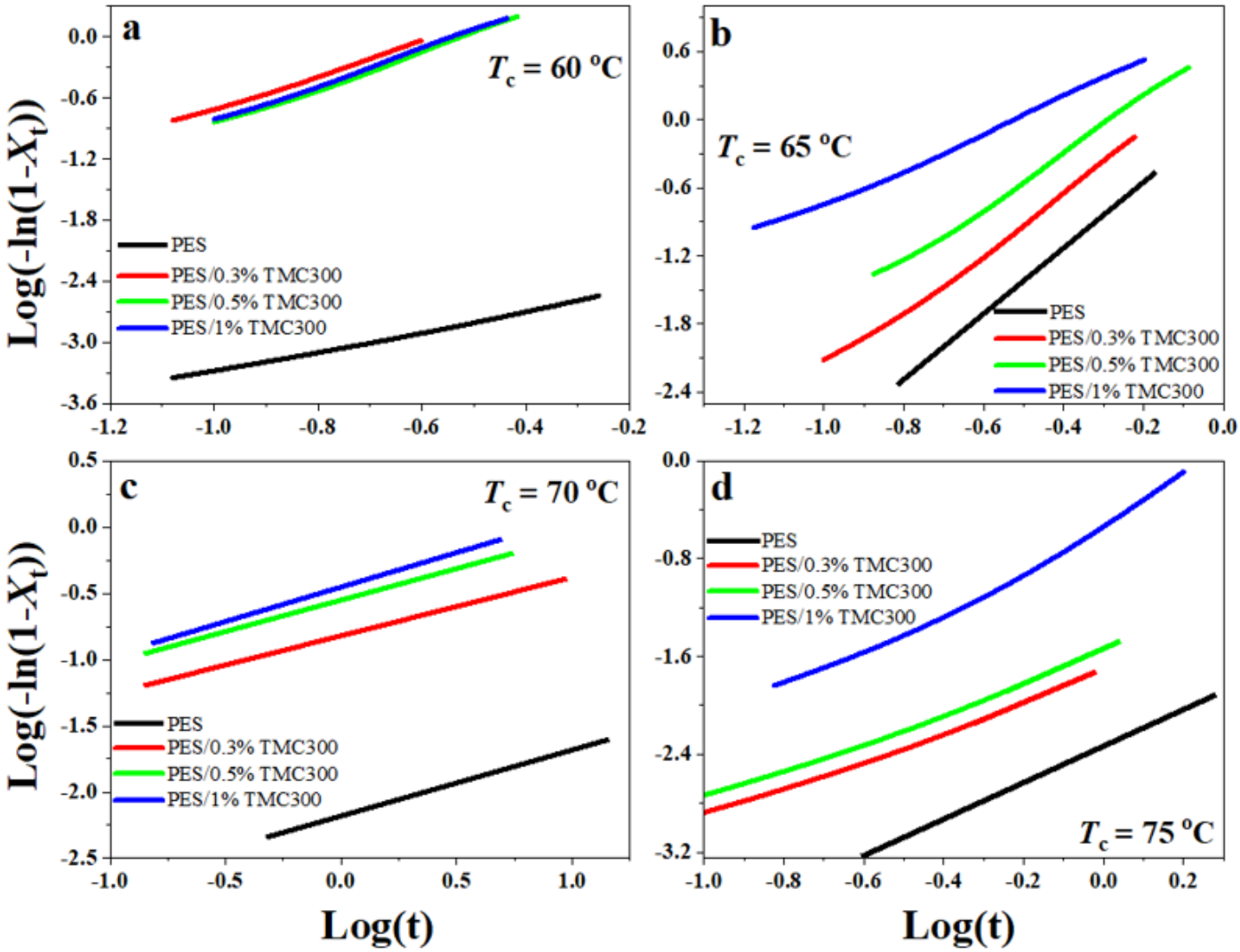

Figure 4

Avrami plots of neat PES and PES/TMC300 at different Tcs

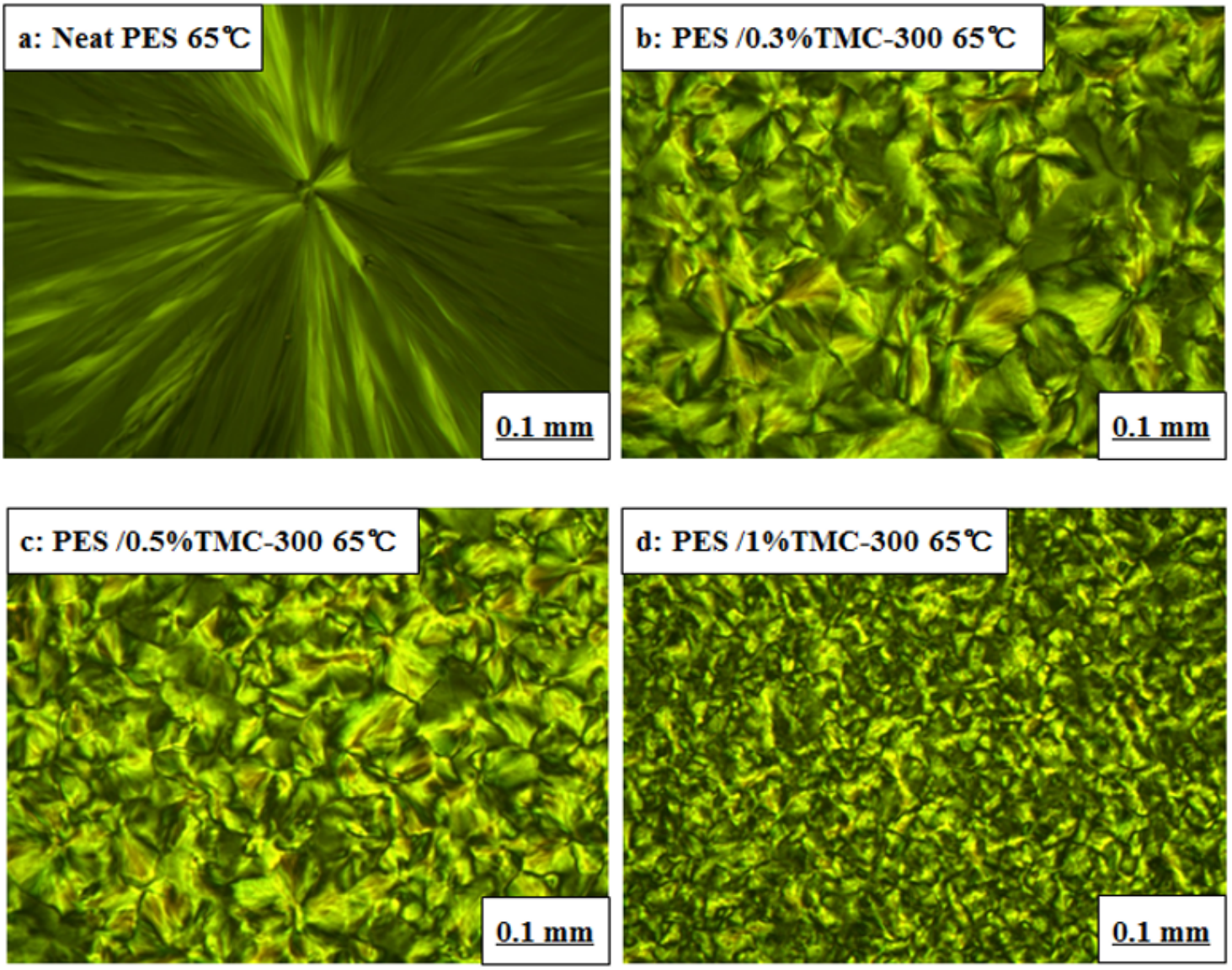

Figure 5

POM images of neat PES and PES/TMC300 at 75 ℃

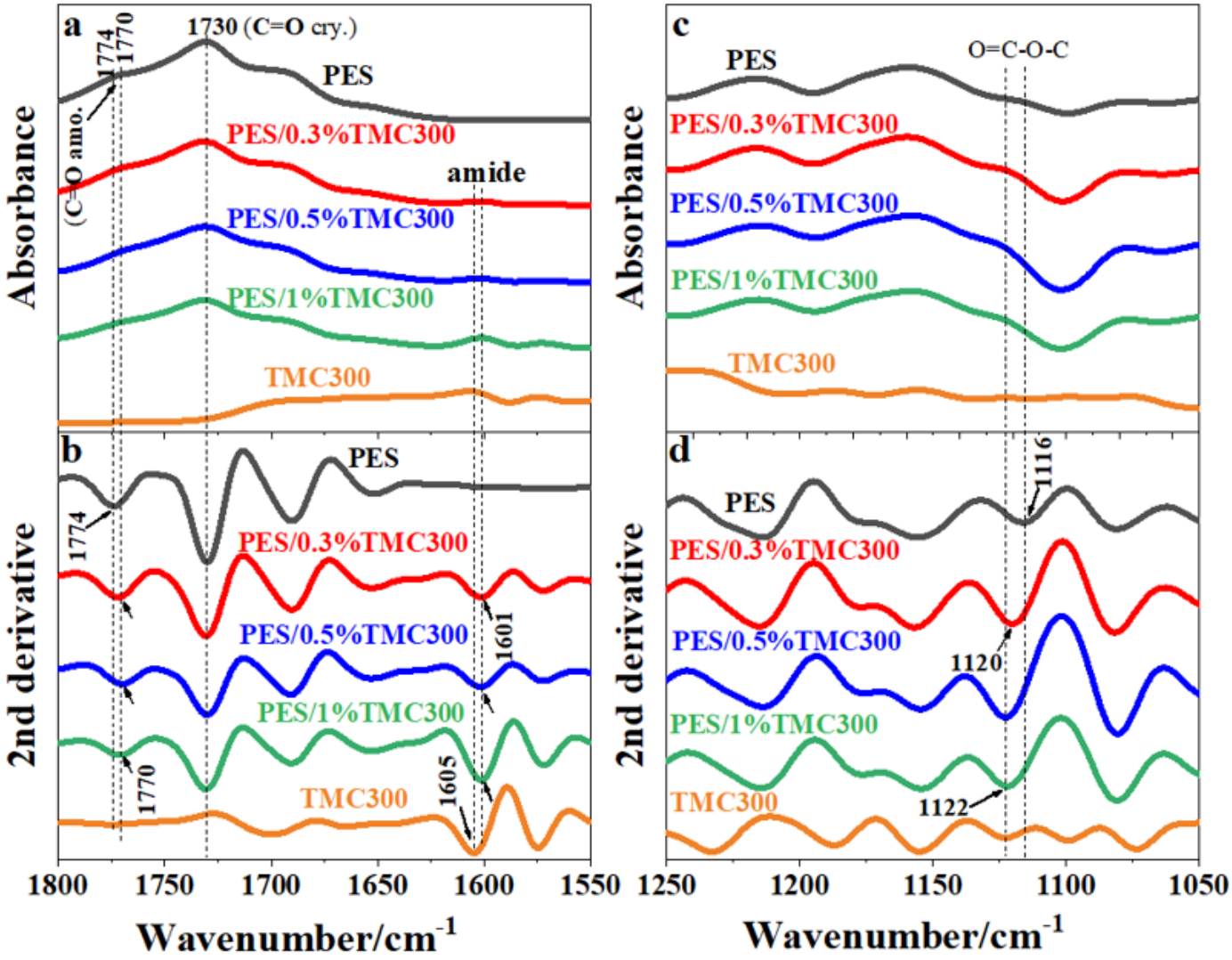

Figure 6

FTIR spectra of neat PES, TMC300 and PES/TMC300 at Tc = 25 °C in two wavenumber regions

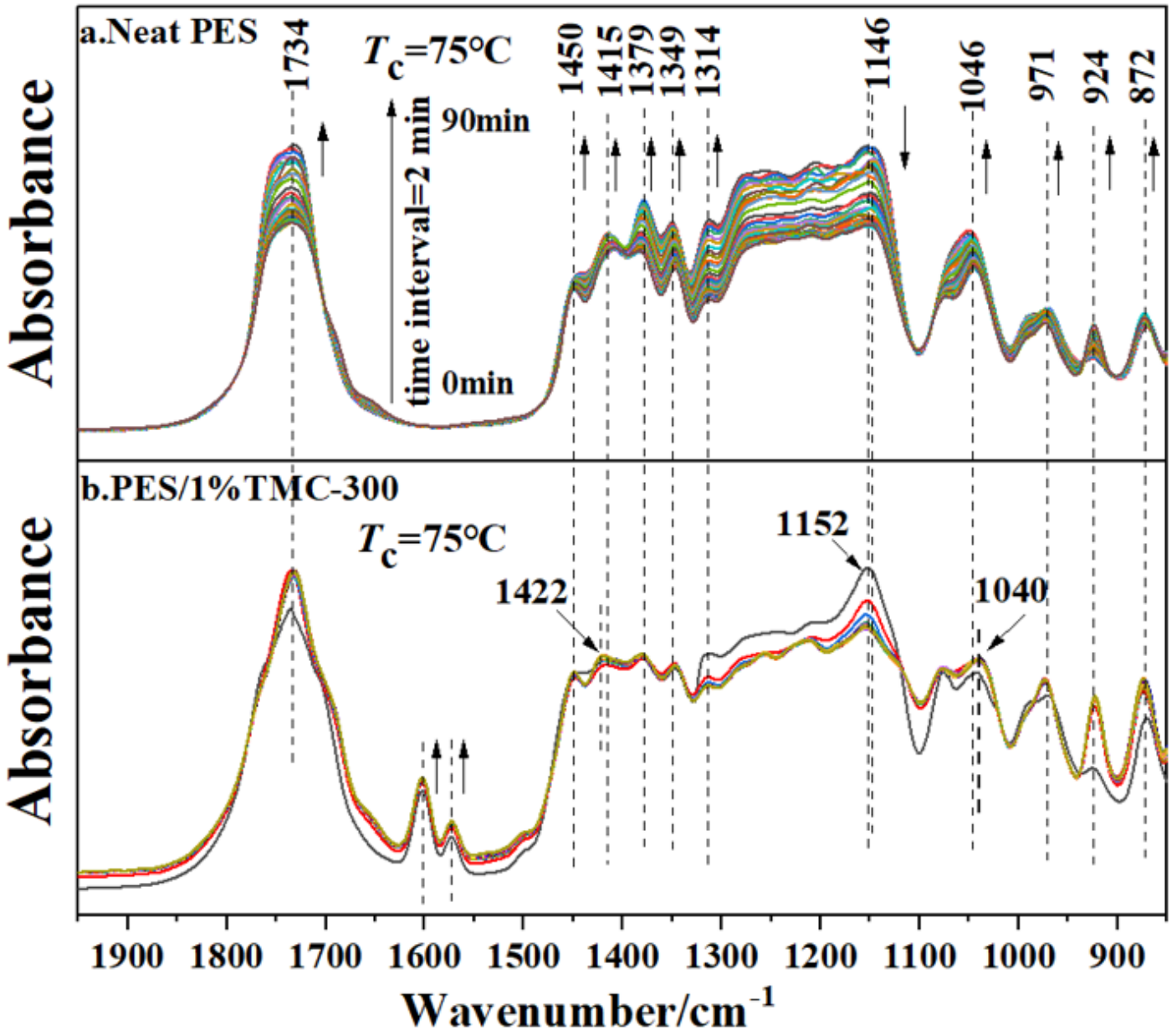

Figure 7

Time-dependent real-time FTIR spectra of neat PES (a) and PES/1%TMC300 (b) collected at 75 °C

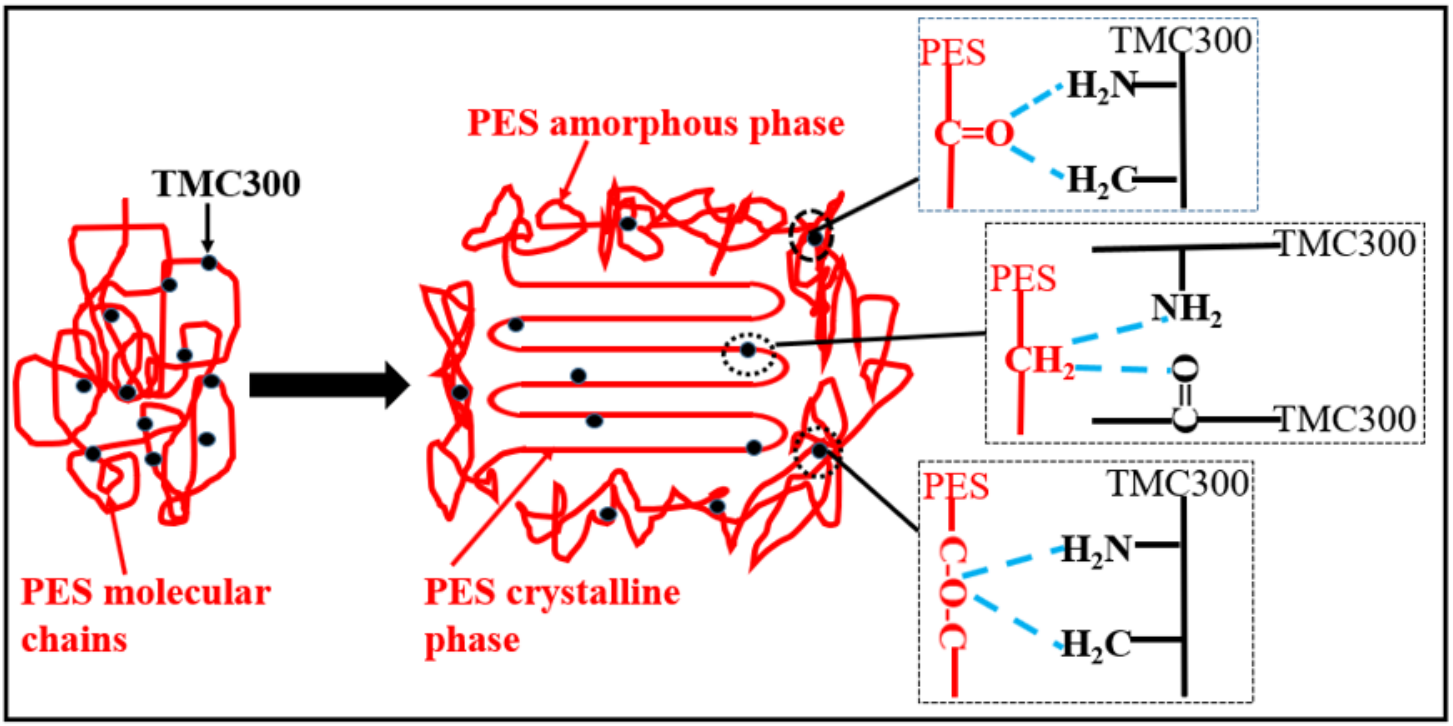

Figure 8

Schematic illustration of hydrogen bond between PES and TMC300

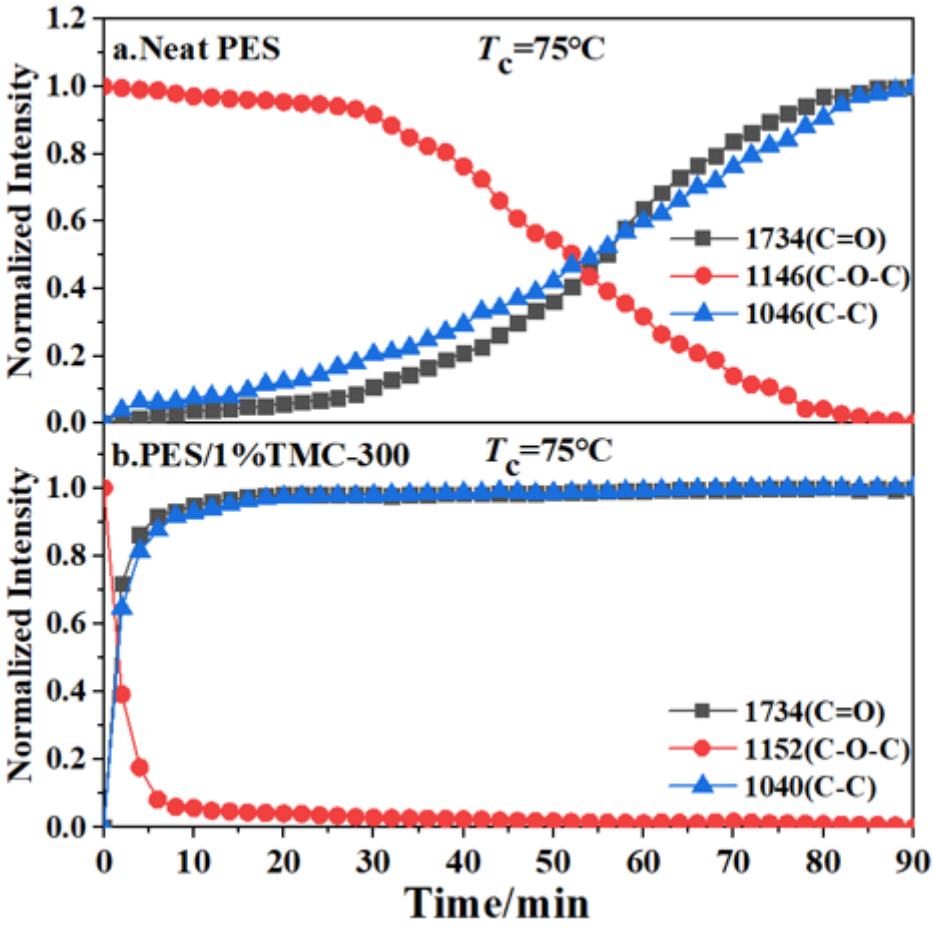

Figure 9

Normalized intensity of several characteristic peaks with crystallization time

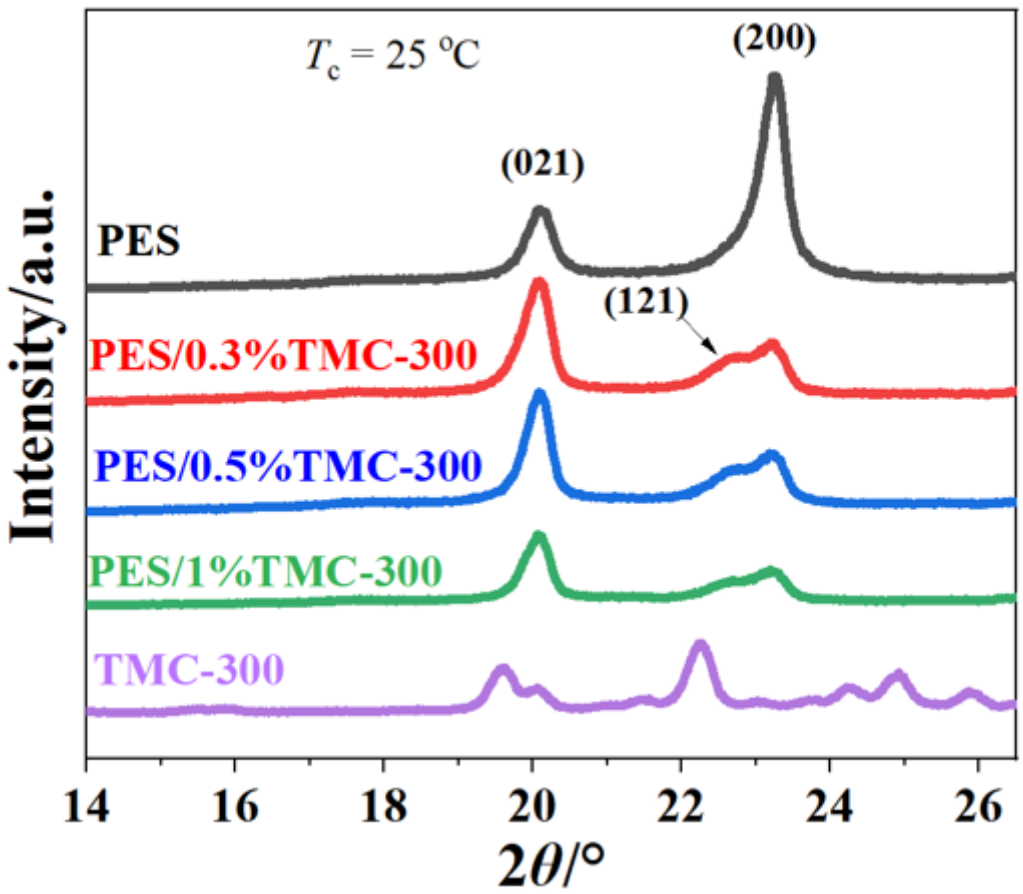

Figure 10

WAXD patterns of neat PES, TMC300 and PES/TMC300 at Tc = 25 °C

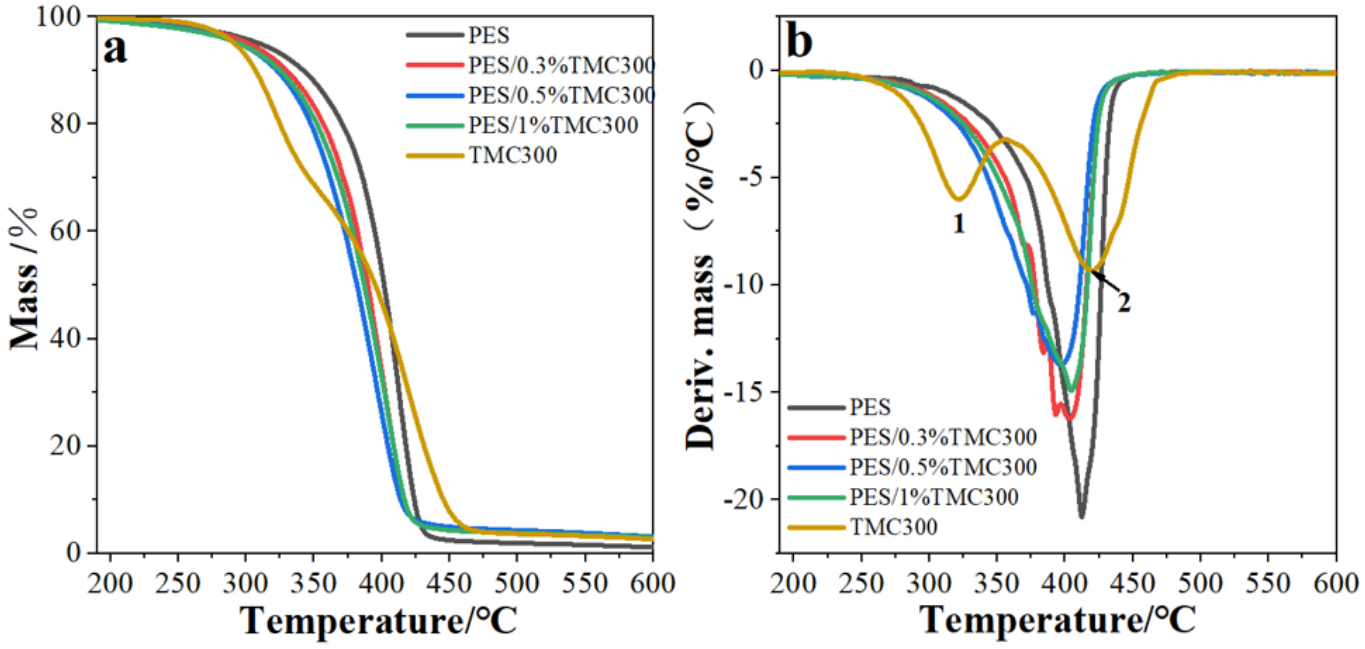

Figure 11

Mass (a) and derivative mass (b) as a function of temperature

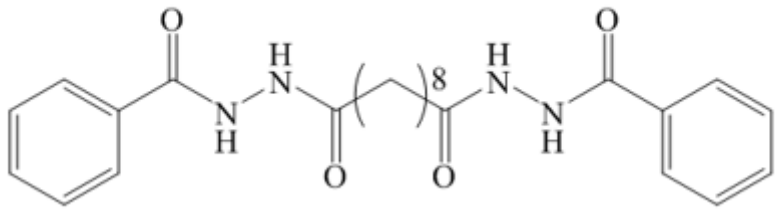

Figure 12

Scheme 1 The chemical structure of the TMC300

Supplementary Files

This is a list of supplementary files associated with this preprint. Click to download.

- SupplementaryMaterial.docx